AJNR

Interventional MR Imaging with an Endospinal Imaging Coil: Preliminary Results with Anatomic Imaging of the Canine and Cadaver Spinal Cord

George Rappard, Gregory J. Metzger, Paul T. Weatherall and Phillip D. Purdy

AJNR Am J Neuroradiol 2004, 25 (5) 835-839
http://www.ajnr.org/content/25/5/835

AJNR Am J Neuroradiol 25:835–839, May 2004

Technical Note

Interventional MR Imaging with an Endospinal Imaging Coil: Preliminary Results with Anatomic Imaging of the Canine and Cadaver Spinal Cord

George Rappard, Gregory J. Metzger, Paul T. Weatherall, and Phillip D. Purdy

Summary: Percutaneous intraspinal navigation (PIN) is a new minimally invasive approach to the subarachnoid space. Using conventional radiographic fluoroscopy, entrance is gained to the lumbar subarachnoid space, allowing navigation throughout the spinal canal. Using an antenna/guidewire introduced via PIN, we performed endospinal MR imaging of the thoracic spinal cord in a cadaver and canine subject. Comparison images were obtained with an optimal surface coil. PIN allows endospinal MR imaging of the spinal cord, providing significant signal-to-noise ratio gains over conventional imaging.

Percutaneous intraspinal navigation (PIN) has been recently described as a minimally invasive approach to the subarachnoid compartment of the spine and brain (1). MR fluoroscopy has been used to guide catheters and guidewires introduced into the CNS through PIN (2, 3), although MR imaging has not yet been applied for interventional imaging of the spinal cord. The purpose of this work was to study the feasibility of anatomic endospinal MR imaging in a cadaver and canine subject.

Description of the Technique

A human cadaver subject was obtained via an institutional willed body program. A live canine subject was obtained following approval from the Institutional Animal Care and Research Advisory Committee. In both subjects, access to the spinal subarachnoid space was obtained as described elsewhere (1). A 100-cm-long, 0.032-inch-diameter loopless antenna/guidewire (Intercept vascular coil; Surgi-Vision, Gaithersburg, MD) was then advanced to the T4 level.

Imaging was performed on a 1.5-T system with 33 mT/m gradient coils. Several sequences of varying resolution were evaluated for endospinal imaging (Table 1). Images obtained with the endospinal coil were compared with images obtained from a linear surface coil. The signal-to-noise ratio (SNR) was determined for the thoracic spinal cord by using both techniques. The SNR was calculated as follows: mean tissue signal intensity/SD noise.

Received June 19, 2003; accepted after revision December 11.

From the Department of Radiology (G.P.), Division of Neuroradiology (G.R., P.D.P.), Philips Medical Systems (G.J.M.), and the Mobility Foundation Center (P.D.P.), the University of Texas Southwestern Medical Center at Dallas, Dallas, TX.

Address correspondence to George Rappard, MD, Department of Radiology, University of Texas Southwestern Medical Center, 5323 Harry Hines Boulevard, Dallas, TX 75390-8896.

Results

The results of comparing SNR in the thoracic spinal cord for the surface coil and endospinal coil are shown in Table 2. Using a fast spin-echo (FSE) T2-weighted sequence of 0.62 mm × 0.62 mm (Fig 1) and 0.39 mm × 0.39 mm resolution (Fig 2), SNR gain with the endospinal coil varied from 193.37% to 164.22%, respectively. Using a steady-state free precession (SSFP) sequence (Figs 3 and 4), a 91.58% SNR gain was seen with the endospinal coil.

High-resolution FSE T2-weighted images of the canine thoracic spinal cord were obtained with the endospinal coil (Fig 5). Using an FSE T2-weighted sequence with a spatial resolution of 0.23 mm × 0.23 mm × 3 mm, anatomic images were obtained with an SNR of 18.03.

Sagittal imaging allowed the exploitation of the cylindrical usable field of view (FOV) available from the endospinal coil (Fig 6). These images well depict paraspinal soft tissues, including nerve roots.

Using the endospinal coil, there is signal intensity inhomogeneity within the FOV with high signal intensity immediately adjacent to the antenna/guidewire and a signal intensity drop-off with increasing distance from the antenna. This signal intensity drop-off is due to decreasing sensitivity with increasing radial distance from the endospinal coil; however, the use of the endospinal coil and a 0.62 mm × 0.62 mm spatial resolution turbo spin factor (TSE) sequence still allowed a 71.15% gain in SNR over the surface coil in portions of the spinal cord most remote from the endospinal coil.

The use of a canine model allowed for the evaluation of degrading artifact due to CSF pulsation. There was no degrading pulsation artifact noted, and cadaver and canine images were similar in quality.

Discussion

Several authors have described the use of an internal coil used for invasive MR imaging. Hurst et al (4) studied the use of various catheter-based coil configurations by using simulations and phantom experiments. In situ (cadaver) and in vivo imaging of canine

TABLE 1: Sequence parameters used in anatomic endospinal imaging

Type	NEX	TR (ms)	TE (ms)	Flip Angle	TSE Factor	Bandwidth (Hz/pixel)	Matrix	Segmental Image	Section Thickness (mm)	FOV	RFOV	SR (mm)
TSE	1	4000	100	90	12	128.9	256 × 256	70%	3	6	70%	0.23 × 0.23
TSE	1	4055.8	100	90	14	144.7	256 × 256	70%	5	10	80%	0.39 × 0.39
TSE	1	1150	110	90	35	375.6	256 × 256	90%	3	16	80%	0.62 × 0.62
SSFP	3	3.7	1.85	55	NA	997.8	192 × 256	50%	15	25	75%	0.98 × 0.98

Note.—TSE = turbo spin echo, SSFP = Steady State Free Precession, FOV = field of view, RFOV = reduced field of view, SR = spatial resolution.

TABLE 2: Comparison of SNR obtained with surface and endospinal coils

	TSE 0.62 mm × 0.62 mm SR	TSE 0.39 mm × 0.39 mm SR	SSFP
Surface coil	22.46	13.5	69.23
Endospinal coil	65.89	35.67	132.63
% SNR gain	193.37	164.22	91.58

iliofemoral arteries were then carried out. Martin and Henkelman (5) constructed an opposed solenoid receiver coil and obtained images of the aorta in a series of five pigs. The authors noted that layers within the artery wall could be discerned with this technique. This group later studied the use of an endovascular receiver coil in the imaging of excised human arteries and correlated their findings with histologic analysis. The authors found that MR imaging findings correlated well with histologic findings in normal and diseased arteries (6, 7). Correia et al (8) used a loopless catheter antenna to image isolated segments of 11 thoracic human aortas. Intravascular MR imaging was compared with surface coil MR imaging and histopathologic analysis of atherosclerotic plaque composition. Botnar et al (9) recently demonstrated the feasibility of in vivo endovascular coronary artery imaging in a swine model by using a loopless antenna. Compared with a surface coil, the authors noted a 70% improvement in SNR 5 mm from the vessel center. The use of the loopless/antenna guidewire design for neurologic imaging has been described elsewhere by Rappard et al (2) in the setting of MR-guided intracranial navigation, in which the device was used as an actively tracked guidewire, capable of simultaneous fluoroscopic brain imaging. The

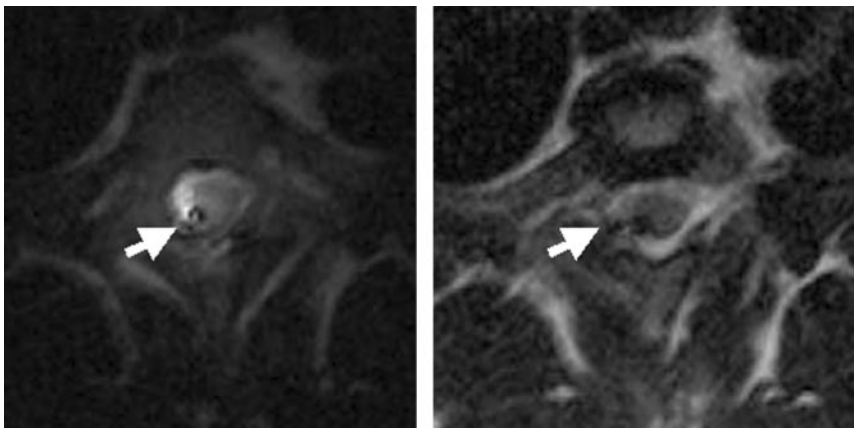

FIG 1. Axial FSE T2-weighted images of the canine spinal cord obtained at the T4 level (acquisition, 1; TR/TE/flip angle, 1150/110/90°; TSE factor, 35; bandwidth, 375.6 Hz; matrix, 256 × 256 with 90% Fourier in phase [90% image]; section thickness, 3 mm; spatial resolution, 0.62 mm × 0.62 mm and FOV, 16 cm with a reduced field of view [RFOV] of 80% obtained with the endospinal coil [*left*] and a surface coil [*right*]). Note the presence of higher cord signal intensity in the endospinal coil images. *Arrow* denotes artifact from the endospinal coil.

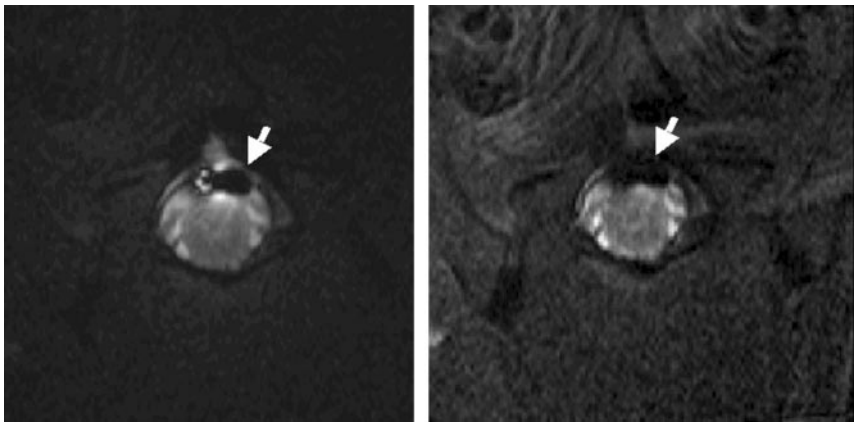

FIG 2. Axial FSE T2-weighted images of a cadaver spine obtained at the T4 level (acquisitions, 1; TR/TE/flip angle, 4055.8/100/90°; TSE factor, 14; bandwidth, 144.7 Hz; matrix, 256 × 256 with 70% image; section thickness, 5 mm; spatial resolution, 0.39 mm × 0.39 mm; and FOV, 10 cm with RFOV of 80%) obtained with endospinal coil [*left*] and surface coil [*right*]). *Arrow* denotes artifact from the endospinal coil. Although the image obtained with endospinal coil has smaller usable FOV, there is greater calculated SNR of the spinal cord.

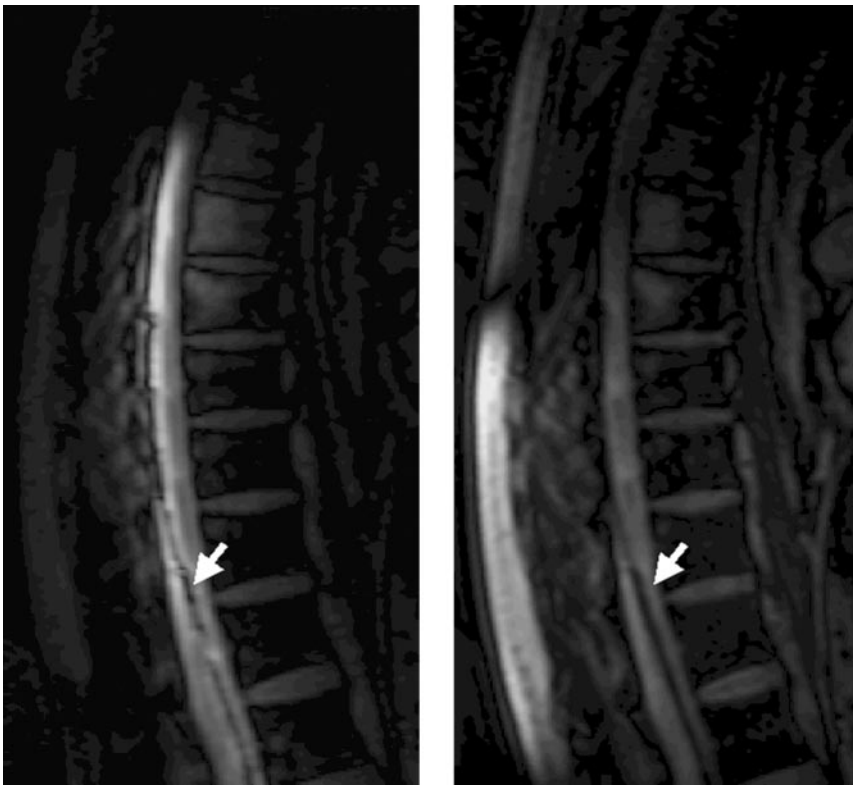

FIG 3. Sagittal SSFP imaging of the cadaver spine (acquisitions, 3; TR/TE/flip angle, 3.7/1.85/55°; bandwidth, 997.8 Hz; matrix, 192 × 256 with 50% image; projection slab, 15 mm; spatial resolution, 0.98 mm × 0.98 mm; and FOV, 25 cm with RFOV of 75% performed with endospinal coil [*left*] and surface coil [*right*]). *Arrow* denotes the endospinal coil positioned within the spinal canal. Note the greater presence of signal intensity available within the spinal canal in the endospinal coil images. Increased CSF signal intensity in endospinal coil image improves cord delineation.

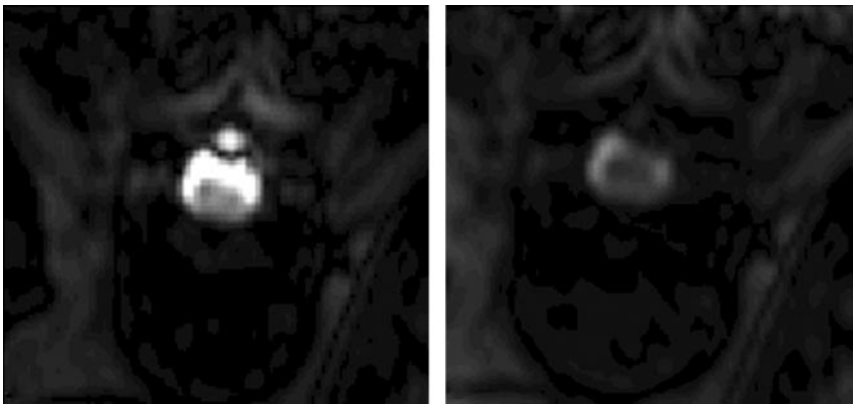

FIG 4. Axial SSFP images of the cadaver spine obtained at the T4 level (acquisitions, 3; TR/TE/flip angle, 3.7/1.85/55°; bandwidth, 997.8 Hz; matrix, 192 × 256 with 50% image; projection slab, 15 mm; spatial resolution, 0.98 mm x 0.98 mm; and FOV, 25 cm with RFOV of 75%). Note the significantly greater amount of canal and cord signal intensity present with the endospinal coil (*left*) versus the surface coil (*right*).

use of a similar device in the setting of endospinal imaging has not been reported.

The loopless antenna/guidewire used in this experiment is a 0.032-inch-diameter nickel-titanium alloy (nitinol)–based receiver and transmit coil (Fig 7). The antenna is 8 cm in length and is attached to a coaxial cable, giving a total length of 100 cm. The active portion of the guidewire is sensitive to signal intensity along its entire length. The antenna consists of two parallel conductors, connected at one end, lying in a dielectric medium and forming a dipole antenna. Tuning, matching, and decoupling circuits are placed outside of the guidewire on the proximal end of a coaxial cable, allowing a small antenna diameter. Sensitivity of the loopless antenna is greatest when the antenna is oriented parallel to the main external magnetic field (10).

High-resolution imaging of the spinal cord has been difficult to achieve with adequate image quality because of the limitations of decreasing signal intensity with decreasing voxel size. The substantial SNR gains seen in endospinal MR allow some of that SNR to be traded for higher spatial resolution. As a result, high-resolution endospinal MR images can be obtained with SNR in the range of conventional resolution images. It should be noted that the sequences used in this study were not optimized to distinguish gray matter from white matter. Rather, the goal was to obtain anatomic images in a reasonable amount of time that could be used for purposes of comparing SNR. In fact, with the exception of the ultrafast SSFP sequence, only one excitation was used. Though not demonstrated here, the superior SNR of the endospinal coil would be expected to produce improved gray-white matter distinction to conventional imaging with the use of an optimized sequence and within the

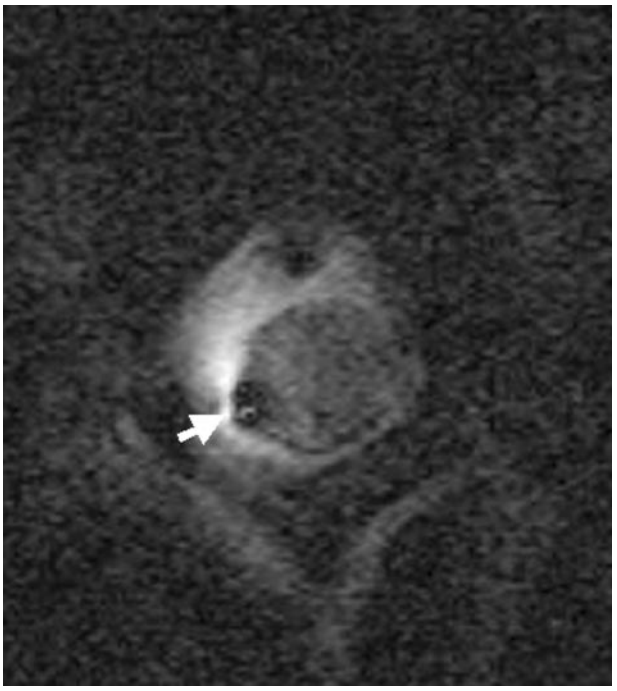

FIG 5. Axial high-resolution FSE T2-weighted image of the canine cord obtained at the T4 level (acquisitions, 1; TR/TE/flip angle, 4000/100/90°; TSE factor, 12; bandwidth, 128.9 Hz; matrix, 256 × 256 with 70% image; section thickness, 3 mm; spatial resolution, 0.23 mm × 0.23 mm; and FOV, 6 cm with RFOV of 70%) obtained with endospinal coil. *Arrow* denotes artifact from endospinal coil in dorsal subarachnoid space.

usable FOV. One caveat is that, because of the high signal intensity immediately adjacent to the coil, saturation effects can occur, limiting contrast. This has been overcome experimentally with the use of a sensitivity-correction algorithm (9).

Comparison was made with a C3 linear surface coil because it was thought that its performance would approach the ideal SNR achievable with available surface coils for imaging of the canine spinal cord. The ideal coil will possess a radius equal to the coil-cord distance. The radius of the opening in the C3 coil is 5.5 cm in diameter, similar to the 5–6-cm depth of the cadaver and canine cord from the surface of the skin at the thoracic level. While not available, a similar-sized quadrature coil would increase signal intensity only by the square root of 2, still falling significantly short of the endospinal coil. Phased array coils were not used because our region of interest was small enough to negate the advantage of added coverage of the phased array.

Although the endospinal coil demonstrated improved image quality while obtaining high-resolution images, what constitutes adequate image quality is yet to be determined. Further study is required to determine threshold contrast and SNR required for detection of pathologic conditions of the cord. We expect to apply the endospinal imaging technique to a canine model of spinal cord injury (11) to obtain useful information on endospinal imaging of cord edema and contusion. Such experiments are expected to prove useful in establishing a balance between resolution, SNR, and contrast-to-noise ratio when optimizing a sequence for use with the endospinal coil. In addition, our group is conducting ongoing work to exploit the high SNR of the endospinal coil for MR spectroscopy and diffusion-weighted imaging of the spinal cord.

We are able to demonstrate the acquisition of high SNR and high-resolution anatomic images of the spinal cord by use of an endospinal coil. Endospinal MR imaging represents a unique potential opportunity for neurointerventional MR imaging and PIN, especially when one considers that the endospinal coil may also serve as a guidewire during spinal procedures. Although our initial results are promising, future work is required to determine threshold resolution, contrast, and SNR needed to detect various diseases of the spinal cord, as well as the applicability of advanced MR methods to endospinal MR imaging. This will be the focus of future investigation.

Acknowledgments

We wish to acknowledge Susan L. Miller, Christina E. Adams, Donna L. Baer, Brian P. Giles, and Ingmar Viohl for technical assistance and Leslie Mihal and Terri Tabaniag for assistance with the preparation of this manuscript.

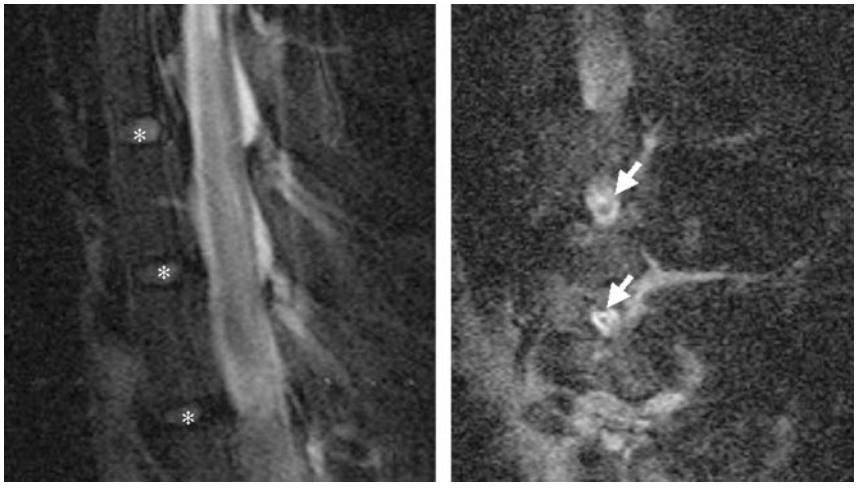

FIG 6. Sagittal (*right*) and parasagittal (*left*) FSE T2-weighted images of the canine spine (acquisitions, 1; TR/TE/flip angle, 3000/100/90°; TSE factor, 12; bandwidth, 121 Hz; matrix, 256 × 256 with 80% image; section thickness, 3 mm; spatial resolution, 0.39 mm × 0.31 mm; and FOV, 8 cm with RFOV of 70%) obtained with endospinal coil. *Asterisks* denote disk spaces and *arrows* denote neural foramina.

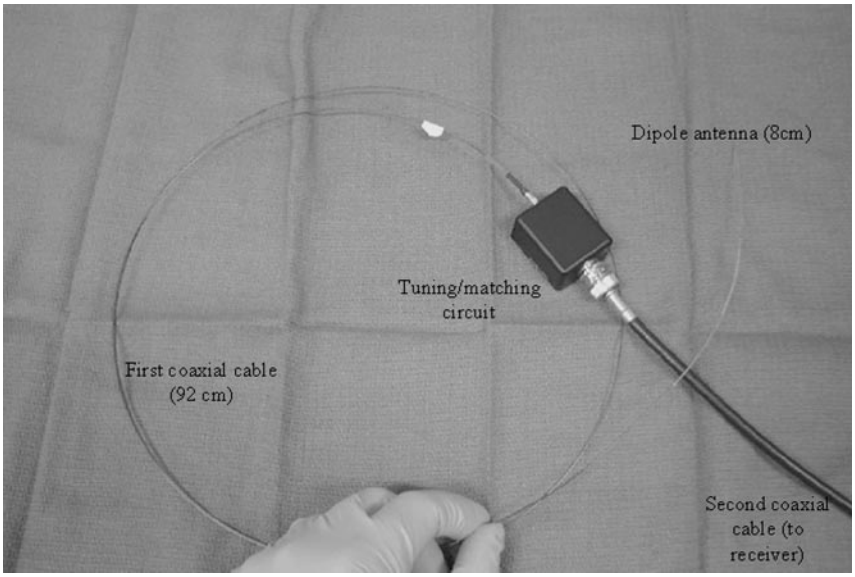

FIG 7. The endospinal coil used in this experiment is a 0.032-inch loopless antenna/guidewire consisting of an 8-cm-long dipole antenna connected to a 92-cm first coaxial cable. Tuning and matching circuits are external. Second coaxial cable connects the apparatus to MR receiver by means of an adapter.

References

1. Purdy PD, Replogle RE, Pride GL Jr, et al. **Percutaneous intraspinal navigation: feasibility study of a new and minimally invasive approach to the spinal cord and brain in cadavers.** *AJNR Am J Neuroradiol* 2003;24:361–365
2. Rappard G, Metzger GJ, Weatherall PT, et al. **MR-guided intracranial navigation using a loopless antenna/guidewire: preliminary results using simultaneous imaging and active tracking.** Presented at the 88th annual meeting of the Radiological Society of North America, December 1–6, 2002, Chicago, IL.
3. Rappard G, Metzger GJ, Fleckenstein JL, et al. **MR-guided catheter navigation of the intracranial subarachnoid space.** *AJNR Am J Neuroradiol* 2003;24:626–629
4. Hurst GC, Hua J, Duerk JL, Cohen AM. **Intravascular (catheter) NMR receiver probe: preliminary design analysis and application to canine iliofemoral imaging.** *Magn Reson Med* 1992;24:343–357
5. Martin AJ, Henkelman RM. **Intravascular MR imaging in a porcine animal model.** *Magn Reson Med* 1994;32:224–229
6. Martin AJ, Gotlieb AI, Henkelman RM. **High-resolution MR imaging of human arteries.** *J Magn Reson Imaging* 1995;5:93–100
7. Martin AJ, Ryan LK, Gotlieb AI, et al. **Arterial imaging: comparison of high-resolution US and MR imaging with histologic correlation.** *Radiographics* 1997;17:189–202
8. Correia LC, Atalar E, Kelemen MD, et al. **Intravascular magnetic resonance imaging of aortic atherosclerotic plaque composition.** *Arterioscler Thromb Vasc Biol* 1997;17:3626–3632
9. Botnar RM, Bucker A, Kim WY, et al. **Initial experiences with in vivo intravascular coronary vessel wall imaging.** *J Magn Reson Imaging* 2003;17:615–619
10. Ocali O, Atalar E. **Intravascular magnetic resonance imaging using a loopless catheter antenna.** *Magn Reson Med* 1997;37:112–118
11. Purdy PD, Duong RT, White CL III, et al. **Percutaneous translumbar spinal cord compression injury in a dog model that uses angioplasty balloons: MR imaging and histopathologic findings.** *AJNR Am J Neuroradiol* 2003;24:177–184